Physics and Imaging in Radiation Oncology 19 (2021) 138–144

Contents lists available at ScienceDirect

Physics and Imaging in Radiation Oncology

journal homepage: www.sciencedirect.com/journal/physics-and-imaging-in-radiation-oncology

Original Research Article

Application of an automatic segmentation method for evaluating cardiac structure doses received by breast radiotherapy patients

Jae Won Jung [a,1], Matthew M. Mille [b,1], Bonnie Ky [c], Walter Kenworthy [c], Choonik Lee [d], Yeon Soo Yeom [b], Aaron Kwag [e], Walter Bosch [f], Shannon MacDonald [g], Oren Cahlon [h], Justin E. Bekelman [i], Choonsik Lee [b,*], on behalf of the RadComp Consortium

[a] Department of Physics, East Carolina University, Greenville, NC 27858, United States
[b] Division of Cancer Epidemiology and Genetics, National Cancer Institute, National Institutes of Health, Rockville, MD 20850, United States
[c] Department of Medicine, University of Pennsylvania Perelman School of Medicine, Philadelphia, PA 19104, United States
[d] Department of Radiation Oncology, University of Michigan, Ann Arbor, MI 48109, United States
[e] Department of Neuroscience, Vanderbilt University, Nashville, TN 37240, United States
[f] Department of Radiation Oncology, Washington University, St. Louis, MO 63130, United States
[g] Department of Radiation Oncology, Massachusetts General Hospital, Boston, MA 02114, United States
[h] Department of Radiation Oncology, Memorial Sloan Kettering Cancer Center, New York, NY 10065, United States
[i] Department of Radiation Oncology, University of Pennsylvania Perelman School of Medicine, Philadelphia, PA 19104, United States

ARTICLE INFO

Keywords:
Cardiac structures
Automatic segmentation
Breast cancer
Radiotherapy
Late effects

ABSTRACT

Background and purpose: Quantifying radiation dose to cardiac substructures is important for research on the etiology and prevention of complications following radiotherapy; however, segmentation of substructures is challenging. In this study we demonstrate the application of our atlas-based automatic segmentation method to breast cancer radiotherapy plans for generating radiation doses in support of late effects research.
Material and methods: We applied our segmentation method to contour heart substructures on the computed tomography (CT) images of 70 breast cancer patients who received external photon radiotherapy. Two cardiologists provided manual segmentation of the whole heart (WH), left/right atria, left/right ventricles, and left anterior descending artery (LAD). The automatically contours were compared with manual delineations to evaluate similarity in terms of geometry and dose.
Results: The mean Dice similarity coefficient between manual and automatic segmentations was 0.96 for the WH, 0.65 to 0.82 for the atria and ventricles, and 0.06 for the LAD. The mean average surface distance was 1.2 mm for the WH, 3.4 to 4.1 mm for the atria and ventricles, and 6.4 mm for the LAD. We found the dose to the cardiac substructures based on our automatic segmentation agrees with manual segmentation within expected observer variability. For left breast patients, the mean absolute difference in mean dose was 0.1 Gy for the WH, 0.2 to 0.7 Gy for the atria and ventricles, and 1.8 Gy for the LAD. For right breast patients, these values were 0.0 Gy, 0.1 to 0.4 Gy, and 0.4 Gy, respectively.
Conclusion: Our automatic segmentation method will facilitate the development of radiotherapy prescriptive criteria for mitigating cardiovascular complications.

1. Introduction

Radiation dose delivered to the heart is an important constraint in radiotherapy when the radiation field is covering or near the heart because of concerns about late cardiac complications. Evidence for an increased risk of ischemic heart disease and cardiac mortality has been reported for survivors who received radiotherapy for breast cancer [1–6], Hodgkin lymphoma [7], lung cancer [8], and childhood cancer [9]. The Deep Inspiration Breath-Hold (DIBH) technique or prone setup are sometimes used in combination with multiple segmented fields to

* Corresponding author at: Division of Cancer Epidemiology and Genetics, National Cancer Institute, National Institutes of Health, 9609 Medical Center Drive, Rockville, MD 20850, United States.
E-mail address: Choonsik.lee@nih.gov (C. Lee).
[1] These authors contributed equally to this work.

https://doi.org/10.1016/j.phro.2021.08.005
Received 23 April 2021; Received in revised form 12 August 2021; Accepted 13 August 2021

minimize the radiation dose to the heart, especially for left breast treatment [10]. However, it remains unclear how to best optimize treatments because there are major gaps in knowledge around which specific cardiac structures are at risk and the mechanism of damage [11]. Early studies on cardiac late effects often used mean dose to the whole heart (WH) as a radiation exposure indicator, however, an increasing body of literature [12–16] has underscored the importance of considering more detailed dosimetry in order to pinpoint the specific cardiac structure(s) most associated with late complications.

A clear barrier to progress is that it is challenging to contour cardiac substructures on radiotherapy planning computed tomography (CT) images. As a result, most research to date has compared risk of cardiac outcomes among groups of patients receiving radiotherapy versus no radiotherapy or by laterality of breast irradiation [1–4]. CT-based assessment of cardiac substructure dose has been used for dose–response analysis, but such studies typically have a small number of patients and short follow-up, so may not be sufficiently powered [8]. Larger studies on historic cohorts sometimes include radiation doses [5,6], but the estimates are often based on reconstructions of radiotherapy plans on a surrogate CT of a "typical" patient because individualized images are unavailable.

A number of atlas [17–22] and machine learning-based [23–27] cardiac segmentation methods can be found in the literature to facilitate substructure contouring. However, these methods are often demonstrated on contrast-enhanced cardiac CT angiography or magnetic resonance imaging (MRI) datasets whereas the visibility of cardiac substructures on a radiotherapy planning CT can be considerably worse. To help bridge this gap, we previously developed a method to automatically segment the substructures of the heart using a most-similar atlas approach followed by a B-spline transformation [28]. Our segmentation method has the advantage that it depends only on the pre-contoured whole heart, not the quality of CT images. In the current study we demonstrate how our method can be used to contour cardiac substructures on breast radiotherapy planning CT images to generate radiation doses in support of research on late cardiac complications.

2. Materials and methods

2.1. Patient data from RadComp clinical trial

Following an institutional review board-approved protocol we collected non-contrast radiotherapy planning CT images for a convenience sample of 100 breast cancer patients enrolled in the Radiotherapy Comparative Effectiveness (RadComp) clinical trial (NCT02603341) [29] who received external photon beam radiotherapy in the supine position. We selected 30 of the 100 patients to create a cardiac atlas library for the automatic segmentation method. The remaining 70 patients were used for testing segmentation performance (40 left breast and 30 right breast).

The radiotherapy plans for the RadComp study represent current real-world practice in the United States for patients with a high risk of nodal recurrence in whom the internal mammary nodes (IMNs) are covered. Treating physicians were encouraged to reduce heart and lung exposure as much as possible while maintaining adequate coverage of the clinical target volume (CTV). The dose constraint to the CTV for the IMNs was D90% (minimum absorbed dose received by 90% of the CTV volume) >90% of the prescription and the mean heart dose was constrained to less than 15 Gy. Prescribed doses ranged from 45 Gy to 50.4 Gy in 1.8 Gy to 2.0 Gy fractions [29]. We excluded from our study patients treated with electron boost or bilateral photon treatment. Ten patients in the study were treated using the DIBH technique (all left breast).

Anonymized Digital Imaging and Communications in Medicine (DICOM) data delivered from the RadComp Radiorepository included a non-contrast planning CT, a RTSTRUCT file containing the manual contours of the six cardiac structures, and a RTDOSE file containing a three-dimensional (3D) dose matrix for the total treatment. The in-plane resolution of the planning CT images was between 0.74 and 2.54 mm and the slice thickness ranged from 2 to 3.75 mm.

Two cardiologists manually contoured the WH, left atrium (LA), right atrium (RA), left ventricle (LV), and right ventricle (RV), and left anterior descending artery (LAD) on the images of the 100 patients using an internal cardiac structure atlas created by the RadComp team with reference to the work of Feng et al. [30] and Duane et al. [31]. A number of training sessions were held between an expert cardiac sonographer and level III trained echocardiographer to review the contours. Inter- and intra-observer variation was assessed for a small number of patients (Supplementary Tables 1 and 2). Cardiac contouring then proceeded by single expert sonographer with oversight by the level III echocardiographer.

2.2. Automatic segmentation of cardiac structures

The automatic segmentation applied in the present study was the same as described in our previous publication [28] except that we used the segmentations of 30 RadComp patients as the cardiac atlas library, not diagnostic CT images.

The input to our automatic segmentation method is the contour of the WH which is typically drawn on the CT of breast cancer patients during treatment planning. The 30 heart atlases were individually placed at the center of mass of each patient's WH and linearly scaled to match the WH volume. The scaled atlas (out of 30 possible choices) showing the greatest Dice similarity coefficient (DSC) (a volume overlap index between two volume objects ranging from zero to 100%) for the WH was selected. Next, non-rigid transformation was applied between the selected atlas WH volume mask and the patient WH volume mask (not CT image) by a structure-guided B-spline 3D transformation. The resulting transformation matrix was then applied to the WH and substructures of the selected atlas to produce the segmentation. Finally, the automatic contours were smoothed with a Gaussian kernel before being written to DICOM format for analysis.

2.3. Performance evaluation

We evaluated our automatic segmentation algorithm performance in terms of geometry and dose. Geometric performance was quantified by the DSC and average surface distance (ASD) (the average of all distances between the surfaces of two objects) metrics to compare the manual and automatic structure contours. Dose performance was evaluated by applying the structure masks to the 3D dose matrix and comparing calculated dose for the manual and automatic contours. Linear regression was performed to quantify the strength of correlation between doses calculated using the manual and automatic contours and to identify any systematic differences between the two segmentation methods.

Because the mean dose to the WH has been used as a radiation exposure indicator, linear regression analysis was also performed for correlation plots comparing mean WH dose and mean dose to the substructures (manual contouring). We also evaluated the sensitivity and specificity of the automatic segmentation method for assigning patients to four dose-levels. For the mean dose to atria and ventricles the categories were: 0–3 Gy, 3–6 Gy, 6–9 Gy, >9 Gy. For the mean dose to the LAD the categories were: 0–5 Gy, 5–10 Gy, 10–15 Gy, >15 Gy. For the maximum dose to the LAD the categories were: 0–15 Gy, 15–30 Gy, 30–45 Gy, >45 Gy.

Performance of the automatic segmentation method should be evaluated within the context of the uncertainty in manual segmentation. However, our cardiology team provided only a single consensus contouring of the cardiac substructures. Therefore, we opted to assess the sensitivity in the manually calculated doses upon shifting the structure mask by a nominal distance of 5 mm. A shift of this size (~5 pixels) reasonably simulates the variability in manual contouring, patient setup

error, and/or motion of the heart. As a point of comparison, Levis et al. [32] used ECG-gated contrast-enhanced CT images to analyze the mean displacement of several heart structures over the cardiac cycle and recommended planning margins of 5 mm for the LAD. For each patient we shifted the substructure masks by 5 mm in a randomly selected 3D direction and then recalculated the dose. A total of 100 realizations of this shift were performed and the maximal and minimal observed dose were recorded to define a nominal range of values within which the true mean substructure dose is expected to fall.

3. Results

3.1. Geometric performance

Excellent visual agreement was observed between the automatic and manual contours for most patients (Fig. 1). We found no significant difference in geometric performance with treatment laterality (Supplementary Fig. 1). Therefore, for the geometric performance evaluation we grouped the left and right breast radiotherapy patients together for the geometric performance analysis (Fig. 2). The mean DSC between manual and automatic segmentations across the 70 patients was 0.96 for the WH and 0.65 to 0.82 for the atria and ventricles (Table 1). The mean DSC for the LAD was considerably worse at 0.06. The average ASD was 1.2 mm for the WH, 3.4 to 4.1 mm for the atria and ventricles, and 6.4 mm for the LAD.

3.2. Dose performance

The dose to the heart varied with laterality of treatment with most heart substructures tending to receive a higher dose for left-sided treatment, except for the RA (right-side treatment larger) and LA (similar for left- and right-sided treatment) (Supplementary Fig. 2). Therefore, for the dose evaluation we performed separate analyses for left and right breast radiotherapy. T-testing did not reveal any significant difference (5% significance level) in the mean structure doses for left-sided treatment with and without DIBH so we grouped all left breast patients together for the analysis (Supplementary Fig. 3).

For left breast radiotherapy, the mean absolute difference (percent dose difference) between doses calculated using the manual and automatic contours was 0.2 to 0.7 Gy (9.1 to 14%) for the mean dose to the atria and ventricles, 1.8 Gy (22%) for the mean dose to LAD, and 5.1 Gy (30%) for the maximum LAD dose (Table 2). For right breast radiotherapy, these values were 0.1 to 0.4 Gy (8.5 to 14%) for the mean dose to the atria and ventricles, 0.4 Gy (15%) for the mean dose to LAD, and 0.6 (18%) for the maximum LAD dose.

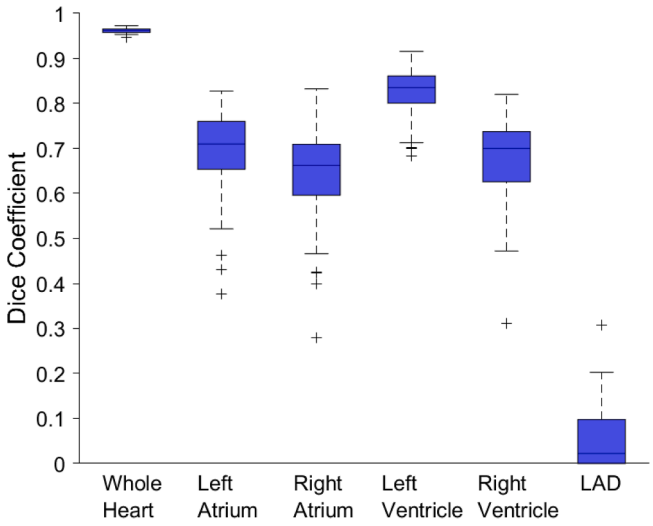

Fig. 2. Box plots of the Dice similarity coefficient (DSC) for the whole heart and substructures for the 70 patients. Outliers are denoted by "+" and are defined as values located 1.5 interquartile ranges below the first quartile or above the third quartile.

The doses calculated using the manual and automatic contours exhibited a high degree of correlation with the lines of best fit for the atria and ventricles having R^2 values >0.87 (Fig. 3). The slopes of the best fit lines for these structures ranged from 0.88 to 1.06 Gy/Gy with y-intercept between −0.10 and 0.52 Gy, demonstrating minimal proportional or constant systematic differences between the two methods. Similar performance was observed for the LAD except in the case of left breast treatment. For left breast radiotherapy, the automatic segmentation method overestimated LAD mean dose with the best fit line having a slope of 0.97 Gy/Gy and y-intercept of 1.13 Gy. For left breast radiotherapy the best fit line for the LAD maximum dose had a slope of 0.93 Gy/Gy and y-intercept of 6.46 Gy. In general, the differences observed between manual and automatic doses for all structures were within expected variability. The confidence intervals for the manual dose estimated from the 5 mm contour shift sensitivity analysis were not

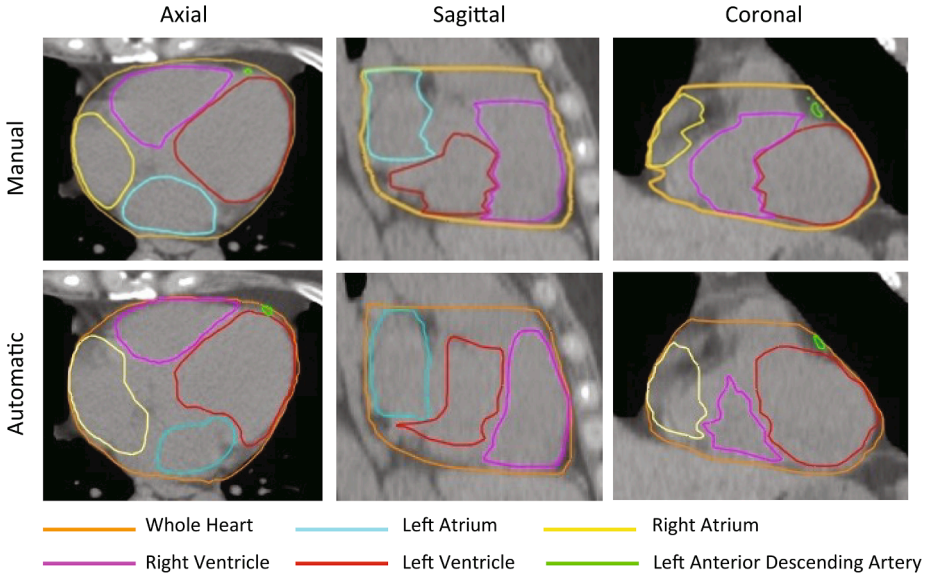

Fig. 1. Comparison of manual (top row) and automatic (bottom row) contours in the axial (left), sagittal (middle), and coronal (right) views.

Table 1
Mean, median, and range of the Dice similarity coefficient (DSC) and average surface distance (ASD) between manual and automatic segmentation averaged over the 70 patients.

Cardiac Structures	DSC			ASD (mm)		
	Mean ± SD	Median	Range	Mean ± SD	Median	Range
WH	0.96 ± 0.01	0.96	0.95–0.97	1.2 ± 0.3	1.2	0.7–1.8
LA	0.69 ± 0.09	0.71	0.38–0.83	3.8 ± 1.5	3.4	1.7–7.8
RA	0.65 ± 0.10	0.66	0.28–0.83	4.1 ± 1.6	3.7	1.5–12.2
LV	0.82 ± 0.05	0.84	0.68–0.92	3.4 ± 1.1	3.0	1.6–7.4
RV	0.68 ± 0.09	0.70	0.31–0.82	4.0 ± 1.2	3.7	1.9–8.2
LAD	0.06 ± 0.07	0.02	0.00–0.31	6.4 ± 2.8	5.7	2.7–15.7

symmetric around the point of estimate and were sometimes sizeable, particularly for the LAD and RV (Table 3).

Linear regression for the correlation plots showing the relationship between mean WH dose (manual contouring) and mean dose to the various substructures (manual contouring) yielded fits for the mean dose to the LA, RA, LV, RV, and LAD which had R^2 values ranging from 0.78 to 0.90 (left breast treatment) and 0.88 to 0.94 (right breast treatment) (Supplementary Figs. 4–8). For the LAD maximum dose the linear regression yielded fits with R^2 values of 0.31 (left breast treatment) and 0.80 (right breast treatment) (Supplementary Fig. 9).

Confusion tables for the dose-level analysis generally exhibited high sensitivity and specificity (>85%) for assigning patients to the selected dose categories (Supplementary Table 3–8).

4. Discussion

In the present study we demonstrated an atlas-based automatic method to segment heart substructures which can be applied to breast radiotherapy planning CT images. The DSC for the atria and ventricles was moderate (0.65 to 0.82). However, the DSC for the LAD was much lower (0.06) because it is a narrow and long structure, making perfect overlap between manual and automatic contours especially challenging to achieve. Despite the observed geometric differences, from the dose performance evaluation we found the doses to the cardiac structures based on our automatic segmentation agreed well with that of manual segmentation within expected variability of manual contouring. Although, the automatic segmentation method did systematically overestimate the mean and maximum dose to the LAD in the case of left breast treatments.

The results of our geometric analysis demonstrate that the performance of our atlas-based automatic segmentation method is comparable to other atlas [17–22] and machine learning-based methods [23–27] found in the literature. However, some methods report better performance with DSCs >0.80 for all four heart chambers. Machine learning methods appear to have an advantage as demonstrated by Morris et al. (2020) [27] who found a significant increase in the DSCs for the coronary arteries compared to their multi-atlas method (DSC ~ 0.50 versus ~ 0.19). Nonetheless, a direct comparison of our results with prior studies is not straightforward because they are mostly demonstrated on contrast-enhanced cardiac CT angiography and MRI datasets [33]. Otherwise, as in the case of Zhou et al. [18], Morris et al. [27], Haq et al. [26], the segmentation methods are applied to non-contrast planning CT images, but use co-registered MRI or contrast-enhanced CT images to assist the manual delineation. In the present study only a non-contrast planning CT was available so there is greater uncertainty in the manual segmentation because the substructures are not always completely visible. Ultimately, the impact of any geometric disagreement on the estimated dose will depend on the gradient of the underlying dose distribution which can vary with factors such as radiotherapy technique and laterality of treatment.

Many studies report significant inter- and intra-observer variability in manual contouring, especially for small structures such as the LAD [18,34]. Zhou et al. [18] reported that the largest ASD for six patients among eight radiation oncologists was 35 mm for the LAD. Our sensitivity analysis showed that even a 5 mm shift in the contours can result in substantial variation in dose, particularly for the RV and LAD for left breast radiotherapy and RA and LAD for right breast radiotherapy. Furthermore, even if the structures are perfectly contoured on CT, the dose estimates would still be limited by patient setup error, patient breathing, and cardiac motion. Given these limitations, our results suggest that further geometric improvement in our automatic segmentation is unlikely to significantly improve the dose estimates.

The sensitivity in the mean dose to the LV, RV, LAD, and maximum LAD dose was greater for left-sided treatments; however, the sensitivity in mean dose to the RA was larger for right-sided treatments and the sensitivity in the mean dose to the LA was independent of treatment

Table 2
Comparison of the cardiac substructure doses between manual and automatic segmentations of a total of 70 breast cancer patients.

Treatment Laterality	Cardiac Structures	Manual Dose (Gy)			Automatic Dose (Gy)			Dose Difference (Gy)*			Mean Dose Difference (%)*
		Mean ± SD	Median	Range	Mean ± SD	Median	Range	Mean ± SD	Median	Range	
Left (n = 40)	WH	4.7 ± 2.5	4.6	1.0–10.5	4.6 ± 2.5	4.5	1.0–10.5	0.1 ± 0.1	0.1	0.0–0.4	1.7
	LA	2.5 ± 1.8	2.4	0.4–7.3	2.5 ± 1.9	2.4	0.3–7.3	0.2 ± 0.2	0.1	0.0–0.7	9.1
	RA	2.6 ± 2.1	2.3	0.3–8.1	2.5 ± 2.1	2.3	0.3–7.9	0.3 ± 0.4	0.1	0.0–1.6	8.7
	LV	4.8 ± 2.2	5.0	1.2–10.4	4.6 ± 2.2	4.7	1.2–9.7	0.3 ± 0.3	0.2	0.0–1.0	5.9
	RV	4.8 ± 2.7	4.6	0.8–11.8	4.7 ± 2.6	4.5	0.8–10.1	0.7 ± 0.7	0.5	0.0–2.6	14
	LAD	9.1 ± 5.1	8.1	2.2–28.0	10.2 ± 5.6	9.4	2.5–25.0	1.8 ± 2.4	1.1	0.0–14.6	22
	LAD_{max}	23.1 ± 11.4	20.7	5.9–49.1	27.8 ± 11.8	25.7	9.3–53.1	5.1 ± 5.0	3.6	0.0–23.4	30
Right (n = 30)	WH	2.9 ± 2.1	2.0	0.6–7.2	2.9 ± 2.1	2.1	0.7–7.1	0.0 ± 0.0	0.0	0.0–0.1	1.0
	LA	2.4 ± 1.9	1.6	0.4–6.4	2.5 ± 2.0	1.7	0.3–7.1	0.2 ± 0.2	0.1	0.0–1.0	8.5
	RA	4.7 ± 2.7	4.2	1.5–11.2	4.7 ± 2.7	4.3	1.0–10.3	0.4 ± 0.3	0.3	0.0–1.2	9.5
	LV	1.5 ± 1.5	1.0	0.2–4.1	1.4 ± 1.2	1.1	0.1–4.2	0.1 ± 0.1	0.1	0.0–0.5	9.2
	RV	3.0 ± 2.3	2.3	0.5–9.8	3.1 ± 2.3	2.6	0.4–10.9	0.3 ± 0.3	0.3	0.0–1.3	14
	LAD	3.0 ± 3.0	1.5	0.3–9.5	2.8 ± 2.9	1.5	0.2–10.7	0.4 ± 0.6	0.2	0.0–2.0	15
	LAD_{max}	4.5 ± 4.6	2.0	0.5–15.7	4.5 ± 4.7	2.1	0.5–15.1	0.6 ± 0.8	0.2	0.0–2.4	18

* Absolute difference between automatic and manual doses.

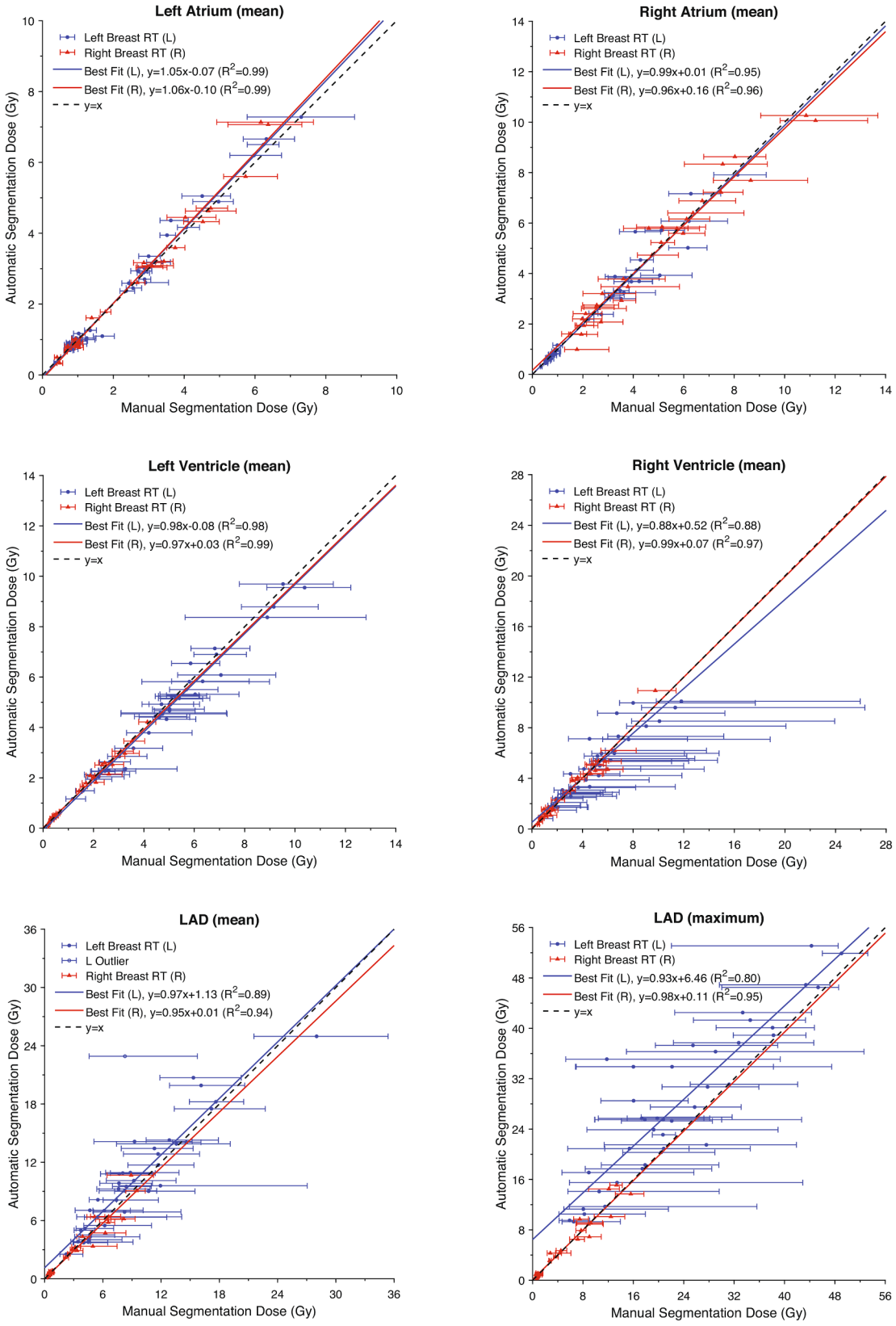

Fig. 3. Correlation plots and best fit lines showing the relationship between manual and automatic segmentation mean doses for the whole heart (WH), left atrium (LA), right atrium (RA), left ventricle (LV), right ventricle (RV), and left anterior descending artery (LAD). The maximum dose to the LAD calculated by each method was also compared. The error bars define the range in dose values observed for 100 realizations of a 5 mm shift in the contours. Best fit lines were calculated separately for left- and right- sided treatment. For the LAD left-sided treatment case, a single outlier was excluded from the linear regression as it was determined to unduly influence the regression.

Table 3
Comparison of sensitivity of cardiac substructure doses to a 5 mm shift in the manual contour. The maximal dose deviation is calculated as the largest deviation in dose observed for 100 realizations of a 5 mm contour shift relative to the dose from manual contouring.

Treatment Laterality	Cardiac Structures	Absolute Maximal Dose Deviation (Gy)			Relative Maximal Dose Deviation (%)		
		Mean ± SD	Median	Range	Mean ± SD	Median	Range
Left (n = 40)	LA	0.3 ± 0.3	0.2	0.0–1.5	15 ± 6	14	6–25
	RA	0.5 ± 0.4	0.2	0.0–1.5	19 ± 6	18	8–38
	LV	1.4 ± 0.7	1.2	0.5–3.9	32 ± 13	28	16–65
	RV	6.1 ± 3.6	6.2	0.9–15.0	129 ± 12	127	108–174
	LAD	4.4 ± 2.4	4.3	1.3–15.1	58 ± 32	45	10–160
	LAD_{max}	13.4 ± 6.9	11.4	2.0–29.5	77 ± 61	56	8–234
Right (n = 30)	LA	0.4 ± 0.4	0.2	0.1–1.5	15 ± 4	15	8–24
	RA	1.2 ± 0.6	1.0	0.5–2.8	30 ± 15	29	11–76
	LV	0.2 ± 0.2	0.1	0.0–0.6	16 ± 6	17	4–26
	RV	0.6 ± 0.5	0.4	0.1–1.7	22 ± 8	22	7–36
	LAD	0.6 ± 0.8	0.2	0.0–2.5	19 ± 9	18	7–51
	LAD_{max}	0.9 ± 1.0	0.4	0.1–3.2	21 ± 18	16	8–98

laterality. For left-sided treatments, the mean dose to the RV was the most sensitive to the 5 mm shift (mean deviation 129%) which can be explained by its larger size in comparison to the LAD. The most sensitive structure for right-sided treatments was the RA (mean deviation 30%) due to its proximity to the field edge. The LAD also exhibited significant variability in mean doses ranging from 10% to 160% (mean 58%) for left-sided treatments and 7% to 51% (mean 19%) for right-sided treatments. The observed sensitivity in the maximum dose to the LAD for left-sided treatment was as high as 234%, suggesting that this dose metric is especially challenging to reliably estimate.

The accuracy requirements of radiation dose estimates for epidemiological research will depend on the size of the health effect being investigated and how the data are analyzed. In some cases, dose is treated as a continuous variable, in which case errors have the effect of widening confidence intervals or altering the slope of a dose–response line depending on whether they are random or systematic in nature. In other cases, patients are assigned to dose-level categories so that dose errors have impact only if they result in misclassification. Our results show that the cardiac substructure doses generated using our automatic segmentation algorithm are suitable for either type of analysis. Overall, the observed correlations between WH dose and substructure dose are slightly worse than that observed in Fig. 3 for the automatic segmentation method, suggesting the automatic segmentation will improve on the approach of using WH as a surrogate for substructure dose.

We acknowledge the following limitations in the current study. First, the application of our method is dependent on the availability of a manual contouring of WH. Second, our structure-guided process only uses the WH for registration and does not consider variations in substructure anatomy between the chosen atlas and patient. Third, we used sensitivity of the substructure doses to a 5 mm shift as a surrogate for variability in manual contouring. This is a useful metric for comparison but is not the same as inter-observer variability. Fourth, in our study we compared doses for automatic and manual contours as reported by the TPS. While useful for evaluating the accuracy of our automatic segmentation method, it is well known that the TPS underestimates dose out-of-field. More accurate dose estimates can be achieved using Monte Carlo radiation transport methods [35].

In summary, we demonstrated an automatic method for segmenting cardiac substructures on breast radiotherapy planning CT images. In the future we plan to apply our method to large patient datasets in support of epidemiological research on cardiac morbidity following radiotherapy.

Declaration of Competing Interest

The authors declare the following financial interests/personal relationships which may be considered as potential competing interests: Dr. Bekelman reports grants from Pfizer, grants from UnitedHealth Group, grants from Embedded Healthcare, grants from Blue Cross Blue Shield of North Carolina, personal fees from UnitedHealthcare, personal fees from CMS, personal fees from NCCN, personal fees from Optum, personal fees from CVS Health, personal fees from Astrazeneca (indirect via NCCN), outside the submitted work.

The other authors have no conflicts of interest to report.

Acknowledgement

This research was funded by a Patient-Centered Outcomes Research Institute (PCORI) Award (PCS-1403-12804) and the intramural research program of the United States National Institutes of Health (NIH), National Cancer Institute, Division of Cancer Epidemiology and Genetics. The contents are solely the responsibility of the authors and do not necessarily represent the official views of the PCORI, its Board of Governors or Methodology Committee, or the NIH.

Appendix A. Supplementary data

Supplementary data to this article can be found online at https://doi.org/10.1016/j.phro.2021.08.005.

References

[1] Darby SC, McGale P, Taylor CW, Peto R. Long-term mortality from heart disease and lung cancer after radiotherapy for early breast cancer: prospective cohort study of about 300 000 women in US SEER cancer registries. Lancet Oncol 2005;6:557–65. https://doi.org/10.1016/S1470-2045(05)70251-5.
[2] Correa CR, Litt HI, Hwang W-T, Ferrari VA, Solin LJ, Harris EE. Coronary artery findings after left-sided compared with right-sided radiation treatment for early-stage breast cancer. J Clin Oncol 2007;25:3031–7. https://doi.org/10.1200/JCO.2006.08.6595.
[3] Bouillon K, Haddy N, Delaloge S, Garbay J-R, Garsi J-P, Brindel P, et al. Long-term cardiovascular mortality after radiotherapy for breast cancer. J Am Coll Cardiol 2011;57:445–52. https://doi.org/10.1016/j.jacc.2010.08.638.
[4] Nilsson G, Holmberg L, Garmo H, Duvernoy O, Sjögren I, Lagerqvist Bo, et al. Distribution of coronary artery stenosis after radiation for breast cancer. J Clin Oncol 2012;30:380–6. https://doi.org/10.1200/JCO.2011.34.5900.
[5] Darby SC, Ewertz M, McGale P, Bennet AM, Blom-Goldman U, Brønnum D, et al. Risk of ischemic heart disease in women after radiotherapy for breast cancer. N Engl J Med 2013;368:987–98. https://doi.org/10.1056/NEJMoa1209825.
[6] Taylor C, Correa C, Duane FK, Aznar MC, Anderson SJ, Bergh J, et al. Estimating the risks of breast cancer radiotherapy: Evidence from modern radiation doses to the lungs and heart and from previous randomized trials. J Clin Oncol 2017;35:1641–9. https://doi.org/10.1200/JCO.2016.72.0722.
[7] van Nimwegen FA, Schaapveld M, Janus CPM, Krol ADG, Petersen EJ, Raemaekers JMM, et al. Cardiovascular disease after Hodgkin lymphoma treatment: 40-year disease risk. JAMA Intern Med 2015;175:1007. https://doi.org/10.1001/jamainternmed.2015.1180.
[8] Reshko LB, Kalman NS, Hugo GD, Weiss E. Cardiac radiation dose distribution, cardiac events and mortality in early-stage lung cancer treated with stereotactic body radiation therapy (SBRT). J Thorac Dis 2018;10:2346–56. https://doi.org/10.21037/jtd.2018.04.42.
[9] Tukenova M, Guibout C, Oberlin O, Doyon F, Mousannif A, Haddy N, et al. Role of cancer treatment in long-term overall and cardiovascular mortality after childhood

cancer. J Clin Oncol 2010;28:1308–15. https://doi.org/10.1200/JCO.2008.20.2267.
[10] Soumarová R, Rušinová L. Cardiotoxicity of breast cancer radiotherapy - overview of current results. Rep Pract Oncol Radiother 2020;25:182–6. https://doi.org/10.1016/j.rpor.2019.12.008.
[11] Darby SC, Cutter DJ, Boerma M, Constine LS, Fajardo LF, Kodama K, et al. Radiation-related heart disease: Current knowledge and future prospects. Int J Radiat Oncol Biol Phys 2010;76:656–65. https://doi.org/10.1016/j.ijrobp.2009.09.064.
[12] Aznar MC, Korreman S-S, Pedersen AN, Persson GF, Josipovic M, Specht L. Evaluation of dose to cardiac structures during breast irradiation. Br J Radiol 2011;84:743–6. https://doi.org/10.1259/bjr/12497075.
[13] Tan W, Liu D, Xue C, Xu J, Li B, Chen Z, et al. Anterior myocardial territory may replace the heart as organ at risk in intensity-modulated radiotherapy for left-sided breast cancer. Int J Radiat Oncol Biol Phys 2012;82:1689–97. https://doi.org/10.1016/j.ijrobp.2011.03.009.
[14] Wollschläger D, Karle H, Stockinger M, Bartkowiak D, Bührdel S, Merzenich H, et al. Radiation dose distribution in functional heart regions from tangential breast cancer radiotherapy. Radiother Oncol 2016;119:65–70. https://doi.org/10.1016/j.radonc.2016.01.020.
[15] Becker-Schiebe M, Stockhammer M, Hoffmann W, Wetzel F, Franz H. Does mean heart dose sufficiently reflect coronary artery exposure in left-sided breast cancer radiotherapy?: Influence of respiratory gatingSpiegelt die mittlere Herzdosis im Rahmen der Radiotherapie beim linksseitigen Mammakarzinom die Dosisbelastung der Koronararterien ausreichend wider?: Einfluss der Atemtriggerung. Strahlenther Onkol 2016;192:624–31. https://doi.org/10.1007/s00066-016-1011-y.
[16] Milgrom SA, Varghese B, Gladish GW, Choi AD, Dong W, Patel ZS, et al. Coronary artery dose-volume parameters predict risk of calcification after radiation therapy. J Cardiovasc Imaging 2019;27:268. https://doi.org/10.4250/jcvi.2019.27.e38.
[17] Kirisli HA, Schaap M, Klein S, Neefjes LA, Weustink AC, Walsum TV, et al. Fully automatic cardiac segmentation from 3D CTA data: A multi-atlas based approach. Medical Imaging 2010: Image Processing, vol. 7623, International Society for Optics and Photonics; 2010, p. 762305. https://doi.org/10.1117/12.838370.
[18] Zhou R, Liao Z, Pan T, Milgrom SA, Pinnix CC, Shi A, et al. Cardiac atlas development and validation for automatic segmentation of cardiac substructures. Radiother Oncol 2017;122:66–71. https://doi.org/10.1016/j.radonc.2016.11.016.
[19] Finnegan R, Dowling J, Koh E-S, Tang S, Otton J, Delaney G, et al. Feasibility of multi-atlas cardiac segmentation from thoracic planning CT in a probabilistic framework. Phys Med Biol 2019;64:085006. https://doi.org/10.1088/1361-6560/ab0ea6.
[20] Morris ED, Ghanem AI, Pantelic MV, Walker EM, Han X, Glide-Hurst CK. Cardiac substructure segmentation and dosimetry using a novel hybrid magnetic resonance and computed tomography cardiac atlas. Int J Radiat Oncol Biol Phys 2019;103:985–93. https://doi.org/10.1016/j.ijrobp.2018.11.025.
[21] Kaderka R, Gillespie EF, Mundt RC, Bryant AK, Sanudo-Thomas CB, Harrison AL, et al. Geometric and dosimetric evaluation of atlas based auto-segmentation of cardiac structures in breast cancer patients. Radiother Oncol 2019;131:215–20. https://doi.org/10.1016/j.radonc.2018.07.013.
[22] Luo Y, Xu Y, Liao Z, Gomez D, Wang J, Jiang W, et al. Automatic segmentation of cardiac substructures from noncontrast CT images: accurate enough for dosimetric analysis? Acta Oncol 2019;58:81–7. https://doi.org/10.1080/0284186X.2018.1521985.
[23] Mortazi A, Burt J, Bagci U. Multi-planar deep segmentation networks for cardiac substructures from MRI and CT. In: Pop M, Sermesant M, Jodoin P-M, Lalande A, Zhuang X, Yang G, editors. Statistical Atlases and Computational Models of the Heart. ACDC and MMWHS Challenges. Cham: Springer International Publishing; 2018. p. 199–206. https://doi.org/10.1007/978-3-319-75541-0_21.
[24] Payer C, Štern D, Bischof H, Urschler M. Multi-label whole heart segmentation using CNNs and anatomical label configurations. In: Pop M, Sermesant M, Jodoin P-M, Lalande A, Zhuang X, Yang G, editors. Statistical Atlases and Computational Models of the Heart. ACDC and MMWHS Challenges. Cham: Springer International Publishing; 2018. p. 190–8. https://doi.org/10.1007/978-3-319-75541-0_20.
[25] Wang C, Smedby Ö. Automatic whole heart segmentation using deep learning and shape context. In: Pop M, Sermesant M, Jodoin P-M, Lalande A, Zhuang X, Yang G, editors. Statistical Atlases and Computational Models of the Heart. ACDC and MMWHS Challenges. Cham: Springer International Publishing; 2018. p. 242–9. https://doi.org/10.1007/978-3-319-75541-0_26.
[26] Haq R, Hotca A, Apte A, Rimner A, Deasy JO, Thor M. Cardio-pulmonary substructure segmentation of CT images using convolutional neural networks. In: Nguyen D, Xing L, Jiang S, editors. Artificial intelligence in radiation therapy. Cham: Springer International Publishing; 2019. p. 162–9. https://doi.org/10.1007/978-3-030-32486-5_20.
[27] Morris ED, Ghanem AI, Dong M, Pantelic MV, Walker EM, Glide-Hurst CK. Cardiac substructure segmentation with deep learning for improved cardiac sparing. Med Phys 2020;47:576–86. https://doi.org/10.1002/mp.v47.210.1002/mp.13940.
[28] Jung JW, Lee C, Mosher EG, Mille MM, Yeom YS, Jones EC, et al. Automatic segmentation of cardiac structures for breast cancer radiotherapy. Phys Imaging Radiat Oncol 2019;12:44–8. https://doi.org/10.1016/j.phro.2019.11.007.
[29] Bekelman JE, Lu H, Pugh S, Baker K, Berg CD, de Gonzalez AB, et al. Pragmatic randomised clinical trial of proton versus photon therapy for patients with non-metastatic breast cancer: the Radiotherapy Comparative Effectiveness (RadComp) Consortium trial protocol. BMJ Open 2019;9:e025556. https://doi.org/10.1136/bmjopen-2018-025556.
[30] Feng M, Moran JM, Koelling T, Chughtai A, Chan JL, Freedman L, et al. Development and validation of a heart atlas to study cardiac exposure to radiation following treatment for breast cancer. Int J Radiat Oncol Biol Phys 2011;79:10–8. https://doi.org/10.1016/j.ijrobp.2009.10.058.
[31] Duane F, Aznar MC, Bartlett F, Cutter DJ, Darby SC, Jagsi R, et al. A cardiac contouring atlas for radiotherapy. Radiother Oncol 2017;122:416–22. https://doi.org/10.1016/j.radonc.2017.01.008.
[32] Levis M, De Luca V, Fiandra C, Veglia S, Fava A, Gatti M, et al. Plan optimization for mediastinal radiotherapy: Estimation of coronary arteries motion with ECG-gated cardiac imaging and creation of compensatory expansion margins. Radiother Oncol 2018;127:481–6. https://doi.org/10.1016/j.radonc.2018.04.014.
[33] Zhuang X, Li L, Payer C, Štern D, Urschler M, Heinrich MP, et al. Evaluation of algorithms for Multi-Modality Whole Heart Segmentation: An open-access grand challenge. Med Image Anal 2019;58:101537. https://doi.org/10.1016/j.media.2019.101537.
[34] Lorenzen EL, Taylor CW, Maraldo M, Nielsen MH, Offersen BV, Andersen MR, et al. Inter-observer variation in delineation of the heart and left anterior descending coronary artery in radiotherapy for breast cancer: A multi-centre study from Denmark and the UK. Radiother Oncol 2013;108:254–8. https://doi.org/10.1016/j.radonc.2013.06.025.
[35] Mille MM, Jung JW, Lee C, Kuzmin GA, Lee C. Comparison of normal tissue dose calculation methods for epidemiological studies of radiotherapy patients. J Radiol Prot 2018;38:775–92. https://doi.org/10.1088/1361-6498/aabd4f.